Synthesis, Structure, Luminescence, and Raman-Determined Excited State Distortions of a Trinuclear Gold(I) Phosphine Thiolate Complex

Stephen D. Hanna, Saeed I. Khan, and Jeffrey I. Zink*

Department of Chemistry and Biochemistry, University of California, Los Angeles, California 90095

Received October 12, 1995[⊗]

The synthesis, crystal structure and spectroscopic properties of a new luminescent trinuclear gold complex, bis(triethylphosphine)gold(I) [μ-(1,1-dicyanoethylene-2,2-dithiolato-1κS:2$\kappa S'$)][μ-(1,1-dicyanoethylene-2,2-dithiolato-2κS2:3$\kappa S'$)](triethylphosphine-1κP)(triethylphosphine-3κP)triaurate(I), **1**, are reported. The structure contains a linear array of three gold atoms, the central gold on an inversion center. **1** crystallizes in the $P2_1/n$ space group with $a = 13.681(1)$ Å, $b = 11.433(1)$ Å, $c = 15.608(1)$ Å, $\beta = 106.93(1)°$, V=2335.4(3) Å^3, and $Z = 2$. The luminescence spectrum is centered at 19 600 cm^{-1} and displays poorly resolved vibronic structure with a spacing of 470 cm^{-1}, characteristic of a normal mode primarily Au−S in character. The transition is assigned to a dithiolate to gold charge transfer. The vibrational frequencies and intensities obtained from the preresonance Raman spectra are used to calculate the distortions the molecule undergoes when excited to its emissive charge transfer excited state. The largest distortions are along the C═C normal mode centered on the dithiolate ligand and along the Au−S stretching coordinate. These distortions assist in making the charge transfer assignment as dithiolate to gold. The analysis of the emission spectrum and the preresonance Raman spectrum using the time-dependent theory of electronic spectroscopy is discussed.

Introduction

Recently a great deal of research has focused on the study of the synthesis and properties of polynuclear gold(I) phosphines and thiolates.[1−7] Much of this interest has been generated by the clinical use of the mononuclear gold phosphine thiolate complex, auranofin, to treat rheumatoid arthritis.[8] In addition, many of the closed shell d^{10} polynuclear complexes have interesting spectroscopic properties. Many of these compounds are brightly luminescent, [1−3,7] and some display resolved vibronic structure in their emission and/or absorption spectra.[6] The assignment of the emitting state has been a matter of some discussion. In several dinuclear gold bisphosphine complexes the emission has been assigned as a metal centered transition.[1,2d] In several dinuclear gold(I) phosphine thiolates, however, the luminescence has been assigned as a ligand to metal charge transfer, LMCT.[7] Recent studies have confirmed this assignment for $(AuPPh_3)_2$[*i*-MNT].[6]

Our earlier work on the dinuclear gold complex $(AuPPh_3)_2$[*i*-MNT] established that the emission was due to a dithiolate to metal charge transfer based on the bond length changes calculated by using the intensities from the resonance Raman spectrum and the electronic spectrum.[6] Our current studies have focused on exploring the generality of this assignment in related complexes, and on further applying and testing our combined methods of vibrational and electronic spectroscopy and the time dependent theory to assign excited states.[9−11] We have discovered that by using less bulky phosphine groups a trinuclear gold(I) mixed-ligand complex can be synthesized. This new compound is luminescent and has a structured emission spectrum.

In this paper we report the synthesis and crystal structure of a novel trinuclear gold(I) compound, bis(triethylphosphine)gold(I) [μ-(1,1-dicyanoethylene-2,2-dithiolato-1κS:2$\kappa S'$)][μ-(1,1-dicyanoethylene-2,2-dithiolato-2κS2:3$\kappa S'$)](triethylphosphine-1κP)-(triethylphosphine-3κP)triaurate(I), $[Au(PEt_3)_2]^+$ $[Au(AuPEt_3)_2$-$(i\text{-MNT})_2]^-$, **1**, where [*i*-MNT] is the 1,1-dicyanoethylene-2,2-dithiolato ligand and PEt_3 is triethylphosphine. At low temperatures the luminescence spectrum of this complex is structured and contains a progression in a 480 cm^{-1} mode. By examination of the spectroscopic features of this molecule and comparison of them to the properties of the related compounds $(AuPPh_3)_2$[*i*-MNT] and $[n\text{-}Bu_4N]_2^+[Au_2(i\text{-MNT})_2]^{2-}$, the emissive state is assigned. Resonance Raman intensities and the vibronic structure of the emission spectrum are used to calculate excited state distortions. These distortions aid in the assignment of the emitting state.

Experimental Section

Reagents. Carbon disulfide (Mallinckrodt), chloro(triphenylphosphine)gold(I) (Strem), potassium methoxide (Aldrich), silver nitrate (Mallinckrodt) and chloro(triethylphosphine)gold(I) (Strem) were used as received. Methanol (Aldrich) was distilled over calcium hydride. Methylene chloride (Fisher) was distilled over phosphorous pentoxide. Malononitrile (Kodak) was distilled under vacuum prior to use.

⊗ Abstract published in *Advance ACS Abstracts,* August 15, 1996.

(1) King, C.; Wang, J. C.; Khan, M. N. I.; Fackler, J. P., Jr. *Inorg. Chem.* **1989**, *28*, 2145.
(2) (a) Che, C. M.; Wong, W. T.; Lai, T. F.; Kwong, H. L. *J. Chem. Soc., Chem. Commun.* **1989**, 243. (b) Che, C. M.; Kwong, H. L.; Yam, V. W. W.; Cho, K. C. *J. Chem. Soc., Chem. Commun.* **1989**, 885. (c) Yam, V. W. W.; Lai, T. F.; Che, C. M. *J. Chem. Soc., Dalton Trans.* **1990**, 3747. (d) Che, C. M.; Kwong, H. L.; Poon, C. K.; Yam, V. W. W. *J. Chem. Soc., Dalton Trans.* **1990**, 3215.
(3) (a) Schaefer, W. P.; Marsh, R. E.; McCleskey, T. M.; Gray, H. B. *Acta Crystallogr., Sect. C* **1991**, *C47*, 2553. (b) McCleskey, T. M.; Gray, H. B. *Inorg. Chem.* **1992**, *31*, 1733.
(4) Lin, I. J. B; Liu, C. W.; Liu, L. K.; Wen, Y. S. *Organometallics* **1992**, *11*, 1447.
(5) Jaw, H. R. C.; Savas, M. M.; Rogers, R. D.; Mason, W. R. *Inorg. Chem.* **1989**, *28*, 1028.
(6) Hanna, S. D.; Zink, J. I. *Inorg Chem.* **1996**, *35*, 297.
(7) (a) Narayanaswamy, R.; Young, M. A.; Parkhurst, E.; Ouellette, M.; Kerr, M.E.; Ho, D. M.; Elder, R. C.; Bruce, A. E.; Bruce, M. R. M. *Inorg. Chem.* **1993**, *32*, 2506. (b) Jones, W. B.; Yuan, J.; Narayanaswamy, R.; Young, M. A.; Elder, R. C.; Bruce, A. E.; Bruce, M. R. M. *Inorg. Chem.* **1995**, *34*, 1996.
(8) Chaffman, M.; Brogden, R. N.; Heel, R. C.; Speight, T. M.; Avery, G. S. *Drugs* **1984**, *27*, 378.
(9) Lai, D. C.; Zink, J. I. *Inorg. Chem.* **1993**, *32*, 2594.
(10) Wexler, D.; Zink, J. I. *J. Phys. Chem.* **1993**, *97*, 4903.
(11) Wootton, J. L.; Zink, J. I. *J. Phys. Chem.* **1995**, *99*, 7251.

S0020-1669(95)01313-9 CCC: $12.00

Absolute ethanol (Quantum) and anhydrous ethyl ether (Fisher) were used as received.

Synthesis. Potassium 1,1-dicyanoethylene-2,2-dithiolate, K_2[*i*-MNT] and $(AuPPh_3)_2$[*i*-MNT] were synthesized by the literature methods.[12,13] The latter compound was recrystallized by slow diffusion of diethyl ether into a methylene chloride solution of $(AuPPh_3)_2$[*i*-MNT]. Synthesis was confirmed by X-ray powder diffraction.

$[Au(PEt_3)_2]^+[Au(AuP(C_2H_5)_3)_2(i\text{-MNT})_2]^-$, **1**, was synthesized by reacting 2 equiv of nitrato(triethylphosphine)gold(I) with 1 equiv of K_2[*i*-MNT] in a methanol/methylene chloride solution. Chloro(triethylphosphine)gold(I) (0.5 g, 1.43 mmol, Strem Chemicals) was dissolved in a minimum of methylene chloride (Fisher Scientific). To this solution was added 0.242 g (1.43 mmol, Mallinckrodt Chemical) of silver nitrate dissolved in a minimum of methanol. Silver chloride precipitated immediately and was removed by vacuum filtration on a fine frit over celite. The solvent was removed by rotary evaporation to yield a gray/white precipitate. To a methylene chloride solution of the $NO_3AuPPEt_3$ precipitate was added 0.156 g (0.715 mmol) of K_2[*i*-MNT]. The reaction was allowed to stir overnight at room temperature in a loosely stoppered flask that was shielded from the light. The resultant solution was filtered over celite on a medium frit and rinsed with 200 mL of methylene chloride to produce a bright yellow solution. The solvent was removed by rotary evaporation to produce a yellow oil. The oil was dissolved in approximately 2 mL of methylene chloride. Long needlelike crystals were grown from this stock solution by slow diffusion of diethyl ether (Fisher Scientific) into the methylene chloride solution. Crystals were collected and rinsed with diethyl ether. Yield: 0.09 g, 5.84×10^{-5} mol (16%, based on $ClAuPEt_3$) . Anal. Calcd for $Au_4C_{32}H_{60}P_4S_4N_4$: Au, 51.13; C, 24.94; H, 3.93; N, 3.64. Found: Au, 54.53; C, 24.15; H, 3.95; N, 3.33. The elemental analysis was performed by Galbraith Laboratories Inc. IR: ν(C≡N) 2201 cm^{-1}, 2192 cm^{-1} (sharp). Raman: ν(C═C of the [*i*-MNT]) 1390 cm^{-1}, ν(Au—P) 385 cm^{-1}, ν(C≡N) 2201 cm^{-1}.

$[n\text{-}Bu_4N]_2^+[Au_2(i\text{-MNT})_2]^{2-}$ was synthesized using the literature method.[14,15] The compound was recrystallized by slow diffusion of diethyl ether into a methylene chloride solution of $[n\text{-}Bu_4N]_2[Au_2(i\text{-MNT})_2]$. Synthesis was confirmed by Raman spectroscopy (ν(C≡N) 2200 cm^{-1}) and by comparing the emission spectrum to that reported previously.[6]

Spectroscopic Measurements. Luminescence spectra at 20 K were taken using a Spex 1702 single monochromator equipped with a Stanford Research Systems SR400 photon counter and an RCA C31034 photomultiplier tube. The 351 nm line of an Ar ion laser was used for excitation. Data were collected on an IBM PC computer. Solid samples were cooled to 20 K in an Air Products displex closed-cycle helium refrigerator equipped with a thermocouple. All data were corrected for instrument response.

Gated time-resolved emission spectra were recorded on samples held at 77 K in a liquid nitrogen filled quartz dewar. Samples were excited using 406 nm excitation from a XeCl excimer pumped dye laser using DPS dye. Signals were collected using an EG&G Princeton Applied Research gated diode array detector (OMA) and an EG&G Princeton Applied Research Model 1211 high voltage pulse generator. Data collected in this fashion were not corrected for instrument response. Lifetimes were measured at 77 K using the 343 nm excitation from an excimer pumped dye laser. Data were collected using a 0.25 m single monochromator equipped with a 1P28 photomultiplier tube, and a Tektronix RTD-710 transient digitizer. The time constant of the instrument was an order of magnitude smaller than the luminescence lifetime.

Infrared spectra were obtained from KBr pellets on a Nicolet Instruments Model 510P FT-IR spectrometer. Peak locations are accurate to ±5 cm^{-1}.

Raman spectra were taken using a Jobin-Yvon 320/640 triple monochromator equipped with a 256 × 1024 Princeton Instruments liquid nitrogen cooled CCD. Data were collected using an IBM PC computer. Excitation was provided by either a Coherent I90-6 argon ion laser or a Coherent I90-K krypton ion laser. The excitation wavelengths used in these studies were 406.7, 413.1, 457.9, and 514.5 nm. Raman samples were prepared by diluting the compound in powdered KBr to decrease decomposition in the laser beam. Light scattered from the sample was collected at 90° relative to the incident laser beam. Low temperature resonance Raman spectra were taken by cooling samples in a displex closed-cycle helium refrigerator and detecting the scattered light with the apparatus described above. Peak locations are accurate to ±3 cm^{-1}. Resonance Raman intensities were obtained by integrating the peaks numerically and correcting for the self-absorption of the sample using the literature method.[16,17]

Solution absorption spectra were obtained on methylene chloride solutions using a Shimadzu UV260 absorption spectrometer. Quartz cuvettes having a 1 cm path length were used.

X-ray Diffraction Analysis. Light yellow crystals of **1** were grown by slow diffusion of diethyl ether into a concentrated methylene chloride solution at room temperature. A suitable crystal cut to appropriate size (0.35 × 0.12 × 0.11 mm) was mounted on a glass fiber and placed on a modified Picker diffractometer (Crystal Logic) equipped with a liquid nitrogen gas stream low-temperature device and graphite-monochromatized Mo source. Accurate unit cell parameters and orientation matrix were obtained by a least-squares fit to the automatically centered settings of 48 reflections and are listed in Table 3, together with other experimental details. Data were collected at 156 K in the $\theta-2\theta$ scan mode up to a maximum 2θ of 60°. Three intense reflections were monitored every 97 reflections collected and showed no significant variations. Of the 6762 unique reflections measured, 3856 were considered observed ($F > 6\sigma(F)$) and were used in the subsequent structure analysis. Data were corrected for Lorentz, polarization, and absorption effects.

The structure was solved in the monoclinic space group $P2_1/n$ (No. 14) by the heavy atom method. The remaining non-hydrogen atoms were located from subsequent difference-Fourier maps. Except for a disordered methylene group, as noted below, geometrically constrained hydrogen atoms were placed in calculated positions 0.95 Å from the bonded carbon atom and allowed to ride on that atom with fixed temperature factors. A disordered methylene group (C9−C10) was refined with constraints between two conformations, each with an occupancy of half. A total of 234 parameters were refined to final $R = 0.039$ and $R_w = 0.040$. The larger peaks on a final difference electron density map (1.6 e $Å^{-3}$) were near Au. Programs used in this work include locally modified versions of crystallographic programs listed in ref 18.

Results

I. Emission Spectroscopy. All complexes studied are emissive in the solid state at 20 K. All CW emission spectra shown were taken using 351 nm excitation from an argon ion laser and were corrected for instrument response.

$[Au(PEt_3)_2]^+[Au(AuP(C_2H_5)_3)_2(i\text{-MNT})_2]^-$. The low temperature emission spectrum of **1** is shown in Figure 1a. This molecule is brightly luminescent at 20 K and weakly luminescent at room temperature. The 20 K spectrum is broad, having a full width at half the maximum amplitude (fwhm) of 3000 cm^{-1}. The maximum of the luminescence occurs at 19 600 cm^{-1}. The spectrum displays resolved vibronic structure. The vibronic peaks occur at about 21 010, 20 530, 20 060, and 19 610 cm^{-1} with an uncertainty of ±20 cm^{-1}. The average spacing is about 470 cm^{-1}. Careful attempts to purify this compound by repeated recrystallization result in a decrease in

(12) Gompper, R; Topfl, W. *Chem Ber.* **1962**, *95*, 2871.
(13) Khan, M. N. I.; Wang, S.; Heinrich, D. D.; Fackler, J. P., Jr. *Acta Crystallogr., Sect. C* **1988**, *C44*, 822.
(14) Khan, M. N. I.; Wang, S.; Fackler, J. P., Jr. *Inorg. Chem.* **1989**, *28*, 3579.
(15) Khan, M. N. I.; Fackler, J. P., Jr.; King, C.; Wang, J. C.; Wang, S. *Inorg. Chem.* **1988**, *27*, 1672.
(16) Schriver, D. F.; Dunn, J. B. R. *Appl. Spectrosc.* **1974**, *28*, 319.
(17) Womack, J. D.; Mann, C. K.; Vickers, T. J. *Appl. Spectrosc.* **1989**, *43*, 527.
(18) Programs: CARESS (Broach, Coppens, Becker, and Blessing), peak profile analysis, Lorentz and polarization corrections; ABSORB (Coppens, Edwards, and Hamilton), absorption correction calculation; SHELX76 (Sheldrick), full-matrix least-squares refinement; ORTEP (Johnson), figure plotting.

Table 1. Summary of the 20 K Resonance Raman of **1** Using 413.1 nm Excitation[a]

frequency (cm^{-1})	assignment	Savin derived Δ	best fit Δ
380	ν(Au—P)	1.28 ± 0.1	1.22
475	ν(Au—S)	1.20 ± 0.1	1.30
481	ν(Au—S)	1.35 ± 0.1	1.33
606		0.74 ± 0.1	0.80
864	ν(C—S)	0.53 ± 0.05	0.56
1393	ν(C═C)	1.28 ± 0.1	1.18
2201	ν(C≡N)	0.29 ± 0.03	0.29

[a] Assignments of the normal modes are shown along with the distortions (Δ) found from Savin's formula, and the Δ's used in the best fit of the emission spectrum. The errors reflect errors due to experimental uncertainty (see text).

the luminescence intensity at the low energy side of the spectrum and a narrowing of the overall width of the spectrum but also a concomitant loss of the vibronic structure.

Gated emission studies at 77 K of this compound show that the intensity of the low energy side of the luminescence varies substantially with delay. Longer delay times lead to a broadening on the red side of the spectrum. The spectrum that is obtained by using a 1×10^{-5} second delay and a 900×10^{-7} gate width is substantially red shifted and broader than the CW spectrum. The spectrum obtained using short gate widths (1×10^{-8} s) and short delay times (110×10^{-8} s), however, is very similar to the CW spectrum except that the vibronic structure is not resolved at these temperatures. The difference spectrum between short and long delay spectra is similar to the spectrum of K_2[*i*-MNT]. The difference spectrum was fit by a Gaussian which is subtracted from the CW spectrum of **1** in order to obtain the corrected spectrum which is used in our theoretical calculations. The Gaussian was multiplied by a scaling factor (30%) such that the corrected spectrum had the same width as both the narrowest short time gated spectrum and the structureless CW spectrum obtained on samples that had undergone repeated recrystallization.

$(AuPPh_3)_2$[*i*-MNT]. The low temperature (20 K) emission spectrum of $(AuPPh_3)_2$[*i*-MNT] is shown in Figure 1b. The emission spectrum shows well resolved vibronic structure with a progression having a spacing of 480 cm^{-1} and a second progression having a spacing of 1410 cm^{-1}. The spectrum is broad with a full width at half-maximum amplitude (fwhm) of 2000 cm^{-1}, and is asymmetric. The peak maximum occurs at 21 655 cm^{-1}. The emission spectrum of this compound has been reported previously and is included here for the purpose of comparison.[1,6]

$[NBu_4]_2^+[Au_2(i\text{-}MNT)_2]^{2-}$. The low temperature (20 K) emission spectrum of $[NBu_4]_2^+[Au_2(i\text{-}MNT)_2]^{2-}$ is shown in Figure 1c. The spectrum is broad with a fwhm of 2600 cm^{-1}, and is asymmetric. The peak maximum occurs at 19 900 cm^{-1}. This spectrum shows poorly resolved vibronic structure. The emission spectrum of this compound has been reported previously and is included here for comparison purposes.[1,6]

K_2[*i*-MNT]. The 20 K emission spectrum of K_2[*i*-MNT] has been reported previously.[6] Its luminescence spectrum is broad and featureless, having a full width at half-maximum (fwhm) of 5200 cm^{-1}. The peak maximum occurs at 17 400 cm^{-1}.

II. Absorption Spectroscopy. $[Au(PEt_3)_2]^+[Au(AuP(C_2H_5)_3)_2(i\text{-}MNT)_2]^-$. Figure 2 shows the room temperature absorption spectrum of **1** in a methylene chloride solution. The lowest energy absorption maximum occurs at 344 nm and has an extinction coefficient of 61 600 M^{-1} cm^{-1}. No weak lower energy bands could be detected by using concentrated solutions.

III. Resonance Raman Spectroscopy. $[Au(PEt_3)_2]^+[Au(AuP(C_2H_5)_3)_2(i\text{-}MNT)_2]^-$. Preresonance Raman spectra of **1** were obtained in order to assign the vibrations associated with the structure observed in the emission spectrum and to calculate the excited state distortions. Figure 3 shows the 20 K preresonance Raman spectrum of **1** using 413.1 nm excitation. The wavenumber of the modes and the corrected peak areas are given in table 1. The most intense peaks are observed at 2201, 1390, 481, and 475 cm^{-1}. The compound is thermally unstable and low laser powers must be used to prevent sample degradation. Spectra also had to be taken on samples diluted in a KBr matrix in order to inhibit the thermal decomposition of the sample.

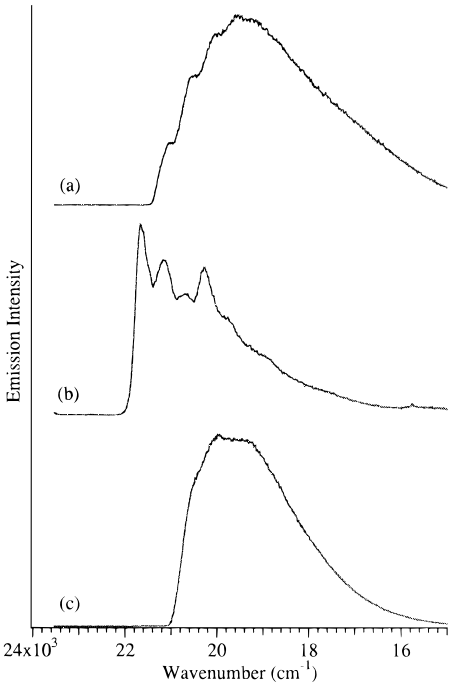

Figure 1. 20 K emission spectrum of (a) $[Au(PEt_3)_2]^+[Au(AuP(C_2H_5)_3)_2(i\text{-}MNT)_2]^-$ and of comparison compounds at 20 K. (b) Emission spectrum of $(AuPPh_3)_2$[*i*-MNT]. (c) Emission spectrum of $[n\text{-}Bu_4N]_2[Au_2(i\text{-}MNT)_2]$. The spectra have been corrected for instrument response.

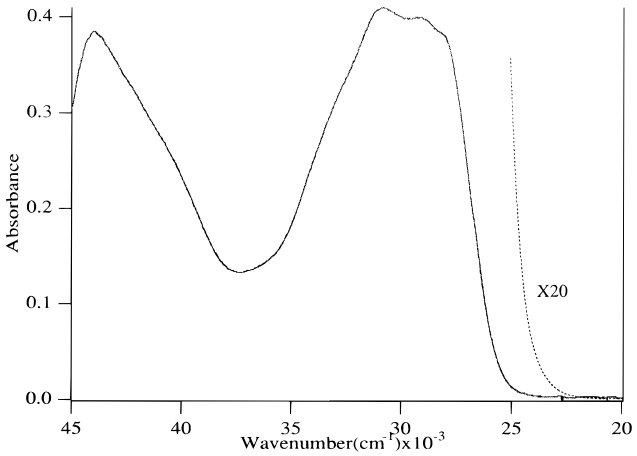

Figure 2. Room temperature methylene chloride solution absorption spectrum of $[Au(PEt_3)_2]^+[Au(AuP(C_2H_5)_3)_2(i\text{-}MNT)_2]^-$.

IV. Crystal Structure of 1. The molecular structure of **1** is shown in Figure 4. Figure 5 shows the packing diagram of the unit cell. The anion is composed of a linear arrangement of three gold atoms. The central gold atom lies on a crystallographic inversion center. Each external gold atom is bridged to the central gold by a single [*i*-MNT] ligand. These gold atoms are capped with a triethylphosphine group in a nearly linear P—Au—S arrangement (∠P—Au—S = 169.8°). The

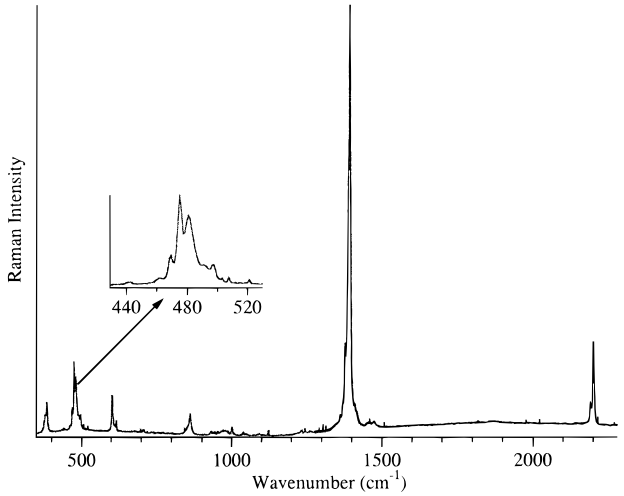

Figure 3. Resonance Raman spectrum of $[Au(PEt_3)_2]^+[Au(AuP(C_2H_5)_3)_2(i\text{-}MNT)_2]^-$ at 20 K. The sample was excited using the 413.1nm line from a Kr ion laser.

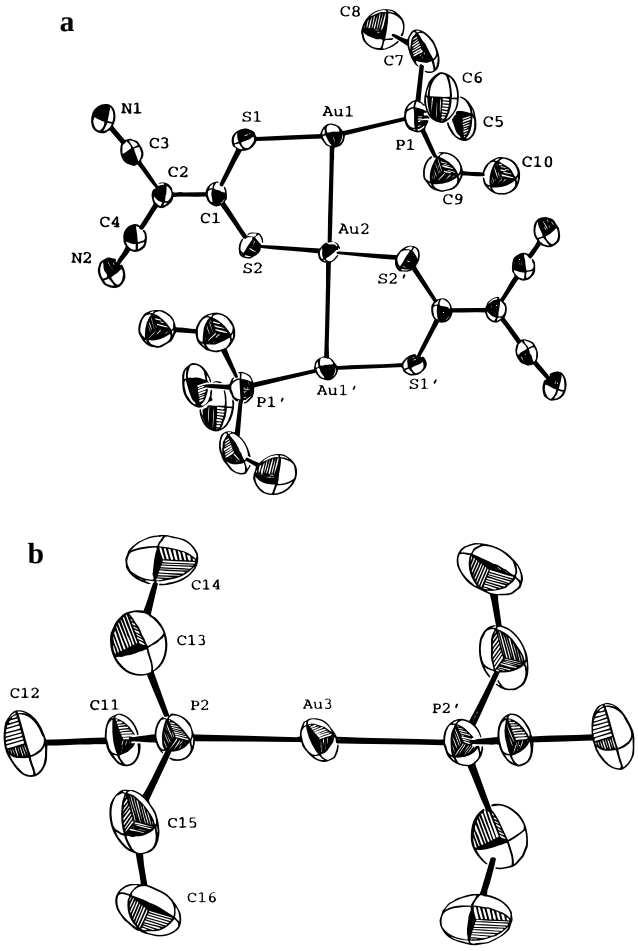

Figure 4. (a) ORTEP drawing of the anion of **1**, $[Au(AuP(C_2H_5)_3)_2(i\text{-}MNT)_2]^-$. (b) ORTEP drawing of the cation of **1**, $[Au(PEt_3)_2]^+$. In both a and b hydrogen atoms have been omitted for clarity.

central gold atom's S−Au−S angle is 180°. These linear arrangements are typical for Au(I) complexes.[19] The gold−gold distances are 3.0 Å which is in the range of gold−gold bonding.[20] Selected bond distances, angles and positional parameters for compound **1** are given in Tables 2−4.

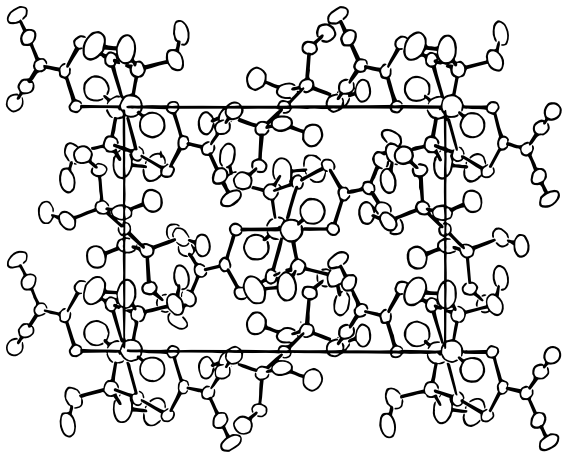

Figure 5. Unit cell of **1**. The "*a*" axis is toward the viewer, and the "*c*" axis is to the right.

Table 2. Crystallographic Data for Compound **1**

fw	1540.85
space group	$P2_1/n$
a, Å	13.681(1)
b, Å	11.433(1)
c, Å	15.608(1)
β, deg	106.93(1)
Z	2
V, Å^3	2335.4(3)
ρ(calcd), g cm^{-3}	2.19
radiation; λ, Å	Mo Kα; 0.7107
abs coeff (μ), cm^{-1}	128.23
temp, K	156
$R = \sum\|\|F_o\| - \|F_c\|/\sum\|F_o\|$	0.039
$R_w = (\sum w(\|F_o\| - \|F_c\|)^2/\sum(\|F_o\|)^2)^{1/2}$	0.040
GOF $= (\sum w(\|F_o\| - \|F_c\|)^2/(N_o - N_v\|)^{1/2}$	1.348

The gold atom of the cation is also located on a crystallographic inversion center and is bound to two triethylphosphine groups. The bonding is linear, having a P−Au−P angle of 180°. Additional information about bond distances, angles and positional parameters can be found in Tables 2−4.

Discussion

I. Interpretation of the Emission Spectrum of 1. The emission maxima of **1** occurs approximately 2000 cm^{-1} to lower energy relative to the emission of the binuclear gold complex $(AuPPh_3)_2[i\text{-}MNT]$. The luminescence of $(AuPPh_3)_2[i\text{-}MNT]$ is due to a LMCT from the dithiolate ligand to the two gold centers. Like $(AuPPh_3)_2[i\text{-}MNT]$, **1** displays resolved vibronic structure having a spacing of 470 ± 20 cm^{-1}. This corresponds to a group mode involving Au−S stretching.[6] On the basis of the energy proximity and the similarity in vibronic spacings in the emission spectrum $(AuPPh_3)_2[i\text{-}MNT]$ to that of **1**, we assign the emission as being a LMCT from dithiolate to gold. This assignment is further corroborated by analysis of the vibronic structure and the resonance Raman intensities of **1** (discussed below).

Based on the σ and π donor properties of the triethylphosphine ligands of **1** we expected that the luminescence of the molecule would be at higher energy than that of $(AuPPh_3)_2[i\text{-}MNT]$. Triethylphosphine is a stronger π and σ donor than triphenylphosphine and should thus interact more strongly with the filled d-orbitals of the Au center.[21] This interaction with the d-orbitals would also cause the gold s and p-orbitals to raise

(19) Puddephatt, H. R. In *Comprehensive Coordination Chemistry*; Wilkinson, G., Gillard, R. D., McCleverty, J. A., Eds.; Pergamon Press; Oxford, England, 1987; Vol. 5, p 861.

(20) Bondi, A. *J. Phys. Chem.* **1964**, *68*, 441. The van der Waals contact is 3.4 Å.

(21) Chang, T. H.; Zink, J. I. *Inorg. Chem.* **1986**, *25*, 2736.

Table 3. Positional Parameters and U_{eq} for the Non-Hydrogen Atoms for Compound **1**[a]

atom	*x*	*y*	*z*	U_{eq}
Au1	0.15467 (3)	0.19268 (4)	0.04130 (3)	0.040
Au2	0.0000	0.0000	0.0000	0.036
S1	0.0643 (2)	0.2616 (2)	0.1357 (2)	0.041
S2	0.0184 (3)	0.0015 (2)	0.1516 (2)	0.050
P1	0.2611 (3)	0.1533 (3)	−0.0423 (2)	0.053
N1	0.0040 (9)	0.3741 (10)	0.3331 (7)	0.075
N2	−0.0859 (9)	0.0149 (9)	0.3425 (7)	0.069
C1	0.0211 (7)	0.1454 (9)	0.1852 (6)	0.035
C2	−0.0085 (7)	0.1695 (8)	0.2617 (6)	0.037
C3	−0.0002 (8)	0.2824 (10)	0.2989 (7)	0.048
C4	−0.0492 (9)	0.0821 (10)	0.3068 (7)	0.051
C5	0.2115 (14)	0.1919 (15)	−0.1593 (9)	0.091
C6	0.1546 (14)	0.3028 (17)	−0.1781 (10)	0.103
C7	0.3776 (11)	0.2343 (20)	−0.0062 (11)	0.105
C8	0.4308 (12)	0.2483 (20)	0.0936 (12)	0.119
C9	0.263 (3)	−0.002 (1)	−0.056 (3)	0.10*
C9′	0.309 (5)	0.008 (2)	−0.017 (4)	0.11*
C10	0.318 (3)	−0.051 (5)	−0.119 (3)	0.09*
C10′	0.301 (5)	−0.099 (5)	−0.078 (6)	0.14*
Au3	0.0000	0.5000	0.0000	0.046
P2	−0.1537 (2)	0.4125 (3)	−0.0691 (2)	0.050
C11	−0.1392 (9)	0.2591 (10)	−0.0786 (8)	0.054
C12	−0.2394 (11)	0.1977 (14)	−0.1297 (10)	0.083
C13	−0.2456 (12)	0.4327 (13)	−0.0085 (10)	0.083
C14	−0.2112 (12)	0.3853 (15)	0.0876 (10)	0.088
C15	−0.2147 (12)	0.4668 (15)	−0.1781 (9)	0.091
C16	−0.1478 (14)	0.4336 (18)	−0.2445 (10)	0.109

[a] Units of U_{eq} are Å^2. An asterisk denotes isotropic refinement. Primed and unprimed atoms of like number are disordered with 50% occupancy each.

Table 4. Selected Interatomic Distances (Å) and Angles (deg) for Compound **1**

Au1−Au2	2.9918(4)	Au1−Au1′	5.9836(6)
Au1−Au3	4.0551(4)	Au2−Au3	5.7164(4)
Au1−S1	2.320(3)	Au1−P1	2.266(3)
S1−C1	1.725(10)	S2−C1	1.724(10)
S2−Au2	2.305(2)	P1−C5	1.808(14)
P1−C7	1.79(2)	P1−C9	1.79(3)
Au3−P2	2.295(3)	P2−C11	1.776(12)
P2−C13	1.796(15)	P2−C15	1.774(14)
Au1−Au2−Au1′	180.00(1)	Au1−P1−C5	114.7(5)
S1−Au1−P1	169.8(1)	Au1−P1−C7	112.3(6)
Au1−S1−C1	109.8(3)	Au1−P1−C9	108.4(15)
S1−C1−C2	117.0(7)	Au3−P2−C11	111.1(4)
S1−C1−S2	125.3(6)	Au3−P2−C13	112.5(5)
C2−C1−S2	117.6(7)	Au3−P2−C15	114.1(5)
C1−S2−Au2	107.8(3)		

in energy, while leaving ligand-centered orbitals relatively unaffected. Thus a ligand to metal charge transfer was expected to shift to higher energy when the phosphine ligand is changed from triphenylphosphine to triethylphosphine . The emission maximum of **1**, however, occurs at lower energy than $(AuPPh_3)_2$-[*i*-MNT]. Comparison of **1** with $[NBu_4]_2^+[Au_2(i\text{-}MNT)_2]^{2-}$ may help to explain this apparent discrepancy.

The emission from $[NBu_4]_2^+[Au_2(i\text{-}MNT)_2]^{2-}$ is very similar to **1**. The spectrum is centered at 19 900 cm^{-1} (vs. 19 600 cm^{-1}), and has a fwhm of 2600 cm^{-1} (vs. 3000 cm^{-1}). The shape of these two spectra are also similar. Both compounds contain S−Au−S linkages, where each sulfur comes from a different [*i*-MNT] ligand. In **1** we have two different types of gold centers. There are two gold atoms which are bound on one side to a sulfur from a dithiolate ligand and on the other to a triethylphosphine. The third gold atom lies on a point of inversion symmetry and is unique. It is bound on both sides to a sulfur from a dithiolate. This unique gold center has a very similar ligand environment to the two gold atoms in $[n\text{-}Bu_4N]_2^+$ $[Au_2(i\text{-}MNT)_2]^{2-}$. Thus, one possible explanation for the lower energy of the electronic transition giving rise to the emission of **1**, similar to that of $[NBu_4]_2^+[Au_2(i\text{-}MNT)_2]^{2-}$, is that there is a large participation of the unique central gold bound to two sulfurs rather than just participation from the golds bonded to both sufur and phosphorus. A second possible analysis is that the interaction between the p-orbitals on the three gold atoms lowers the σ bonding orbital and thus the transition energy.

Analysis of the emission spectrum of **1**, and comparison with the emission of $(AuPPh_3)_2$[*i*-MNT] supports the assignment of the emitting state of **1** as a LMCT from the dithiolates to the gold centers. The similarities of the emissions of $[NBu_4]_2^+$-$[Au_2(i\text{-}MNT)_2]^{2-}$ and **1** suggest that the charge transfer involves large participation of the unique gold center. Below we discuss the analysis of the excited state distortions, i.e. bond length changes that occur in the excited state, and how they aid in the assignment of the emitting state. In the case of **1**, distortions are calculated from resonance Raman intensities and from modeling the vibronic structure observed in the emission spectrum.

II. Analysis of the Excited State Distortions Using Resonance Raman Intensities. A. Assignments. The intensities of peaks observed in the preresonance Raman spectrum of a compound are directly correlated to the magnitudes of the distortion along that normal coordinate in the excited state (see below). The most highly distorted vibrational modes in the charge transfer excited state would be expected to be those on the dithiolate ligand (which is formally oxidized) and the gold−ligand modes because the gold centers are formally reduced. Phosphine-centered distortions should be small.

The bands observed in the Raman spectrum of **1** can be assigned by comparison to the related compounds $(AuPPh_3)_2$-[*i*-MNT], and $[n\text{-}Bu_4N]_2[Au_2(i\text{-}MNT)_2]$ which have many structural features in common to **1**, and have assigned Raman spectra.

The vibrational frequencies of the $[i\text{-}MNT]^{2-}$ ligand can be assigned by comparison with related compounds. The carbon−carbon double bond stretching frequencies in compounds with this ligand generally occur between 1375 and 1432 cm^{-1}.[6,22] In $(AuPPh_3)_2$[*i*-MNT] and $[n\text{-}Bu_4N]_2[Au_2(i\text{-}MNT)_2]$ this mode is observed at 1410 and 1376 cm^{-1} respectively. In **1** the sharp band observed at 1380 cm^{-1} is assigned as the ν(C═C). The C≡N stretching frequency in **1** occurs at 2201 cm^{-1} as is expected based on similar compounds.[22] In $(AuPPh_3)_2$[*i*-MNT] and $[n\text{-}Bu_4N]_2[Au_2(i\text{-}MNT)_2]$ this mode is observed at 2209 and 2200 cm^{-1} respectively. The band observed at 865 cm^{-1} is assigned as the carbon−sulfur stretching frequency of the $[i\text{-}MNT]^{2-}$ ligand. For the related compounds (1,2-dicyanoethylene-1,2-dithiolato)(ethylene)nickel(II), $(AuPPh_3)_2$[*i*-MNT], and $[n\text{-}Bu_4N]_2[Au_2(i\text{-}MNT)_2]$ the ν(C−S) is observed at 866, 865, and 856 cm^{-1} respectively.[6,23,24] While the exact assignment of the mode observed at 606 cm^{-1} is unknown it is attributed to a vibration on the dithiolate ligand because it appears in both of the comparison compounds.

The highly distorted metal−ligand modes are expected to be the gold-phosphorus stretching mode (ν(Au-P)), and the gold−sulfur stretching mode (ν(Au−S)). In the related compounds $(AuPPh_3)_2$[*i*-MNT] and $[n\text{-}Bu_4N]_2[Au_2(i\text{-}MNT)_2]$, the group mode involving Au−S stretching character was observed at 480 and 479 cm^{-1}, respectively.[6] In **1**, we observe two strong peaks in this region. Due to the presence of an inversion center in this molecule only the two symmetric stretches should be

(22) Takahashi, M.; Kano, Y.; Inukai, J.; Ito, M. *Chem. Phys. Lett.* **1992**, *196*, 70.
(23) Clark, R. J. H.; Turtle, P. C. *J. Chem. Soc., Dalton Trans.* **1977**, 2142.
(24) Schläpfer, C. W.; Nakamoto, K. *Inorg. Chem.* **1975**, *14*, 1338.

observed. The bands at 475 and 481 cm^{-1} are assigned as group modes involving the symmetric gold−sulfur stretching component. Weaker satellite peaks are probably the asymmetric combination which become slightly allowed due to crystal defects. In all of the gold phosphine complexes we have studied a strong Raman band is observed at approximately 385 cm^{-1} and is assigned as the gold−phosphorus stretching frequency.[6] This is consistent with that found by other researchers, for mononuclear gold phosphine complexes.[25] Thus the band observed in **1** at 385 cm^{-1} is assigned to be the ν(Au−P). All of these assignments are summarized in Table 1.

B. Calculation of Distortions from Raman Intensities. The intensities of the peaks in the preresonance Raman spectra are related to the normal coordinate distortions that occur in the excited state of a molecule.[26,27] The magnitude of the displacement of the excited state potential energy surface, relative to the ground state surface is related to the intensity of the preresonance Raman band divided by the square of its frequency. For harmonic vibrations the distortions are given explicitly by Savin's formula (eq 1), where $\Delta_k/\Delta_{k'}$ is the

$$\frac{\Delta_k}{\Delta_{k'}} = \left(\frac{I_k \omega_k^{\,2}}{I_{k'} \omega_{k'}^{\,2}}\right)^{1/2} \tag{1}$$

displacement of any mode k relative to that of a reference mode k'. I_k and $I_{k'}$ are the areas of the Raman peaks associated with those modes, and $\omega_{k'}$, and ω_k are the frequency of the modes.[26,27] Equation 1 can be used with the preresonance Raman data to find the displacement of any mode relative to another standard mode. This calculation was performed for **1**, and the results are shown in Table 1. The Savin displacements, Δ_k, are shown along with the assignment of each observed preresonance Raman band. We find that the largest distortions occur in the Au−S group stretching modes, in the ν(Au−P) stretch, and in the ν(C═C) stretch of the dithiolate ligand. These distortions are consistent with a LMCT assignment for the emitting state. The largest distortions are found in the dithiolate ligand and in modes associated with the gold centers to which charge is transferred.

After the relative ratios of the displacements are known, the dimensionless value for the displacement, Δ_k, that was used as a standard can be calculated by using eq 2, where $2\sigma^2$ is

$$2\sigma^2 = \sum_k \Delta_k^{\,2} \omega_k^{\,2} \tag{2}$$

governed by the square of the full width at half-maximum amplitude of the absorption spectrum. The width of an absorption or emission spectrum is related to the sum of the squares of all of the distortions multiplied by the squares of their frequencies.[26,27] Because the lowest energy absorption band overlaps other low energy bands, the fwhm of the emission spectrum was used in eq 2. The distortions calculated from the equations above are given in Table 1.

There are three categories of uncertainties in the calculated distortions. The first category is the experimental uncertainty in measuring peak areas, frequencies, and band widths. The second category includes the assumptions inherent in the Savin formula. These assumptions have been extensively discussed in the literature.[27] The third category involves the properties of the molecule itself such as overlapping absorption bands and closely spaced spin−orbit states. The Savin formula assumes that there is only one excited state. In the case of **1**, however, the emitting state is energetically in close proximity to several other states. For these reasons, the uncertainties in the distortions are larger than the purely experimental uncertainties that are estimated to be ±10%. The calculation of the emission spectrum by using the Raman-determined distortions (section III) provides a test of the accuracy of the distortions. We make use of the facts that the emission spectrum verifies the large Au−S distortion and that the Raman data do not show large distortions in phosphine centered modes in our discussion of the assignments (section IV).

III. Test of the Raman-Determined Distortions Using the Vibronic Structure of the Emission Spectrum. The structure observed in the emission spectrum of **1** was used as an internal check of our previous calculation of the excited state distortions. The structure that is observed in the emission spectrum is indicative of a large distortion in the 480 cm^{-1} mode. The emission spectrum peaks late in the progression (at the fourth quantum) indicating that this mode is highly distorted in the emitting state. This intensity distribution is different from that of the previously studied $(AuPPh_3)_2$[*i*-MNT] whose emission peaked in the first quantum, indicating smaller distortions along both the 480 cm^{-1} mode and the dithiolate ν(C═C) mode at 1410 cm^{-1}.[6] In this similar compound the 480 cm^{-1} peak was assigned as a group mode involving substantial Au−S stretching character. By using the time dependent theory of electronic spectroscopy to fit the emission spectrum, the displacement of the excited state potential energy surface along each normal coordinate can be confirmed.[27−30]

The emission spectrum of **1** can be calculated using the time dependent theory of electronic spectroscopy.[27−30] In the time dependent picture, when a photon is emitted a wave packet, ϕ, is produced on the ground state surface. Since this wave packet results from a vertical transition from the excited state, it is not an eigenfunction of the ground state. The nonstationary wave packet will then evolve in time obeying the time dependent Schrödinger equation. The emission spectrum is determined by the dynamics of the wave packet on the ground state potential energy surface.[27] The emission spectrum is given by

$$I(\omega) = C\omega^3 \int_{-\infty}^{+\infty} \exp(i\omega t)\langle\phi|\phi(t)\rangle \, \mathrm{d}t \tag{3}$$

where $I(\omega)$ is the emission intensity in photons per unit volume per unit time at the frequency ω and C is a constant. The most important part of eq 3 is $\langle\phi|\phi(t)\rangle$, which is the autocorrelation function of the initial wave packet, ϕ, and the wave packet as it evolves in time, $\phi(t)$. The initial wave packet $\phi(t = 0)$ is the lowest energy eigenfunction of the excited state potential energy surface multiplied by the transition dipole moment. Methods for calculating the autocorrelation function have been discussed in the literature.[27−30]

The autocorrelation function depends strongly on the displacement, Δ, of the excited state potential energy surface along a normal coordinate relative to the minimum of the ground state potential energy surface. Changes in the values of the displacement along a normal coordinate will alter the intensity distribution in a calculated spectrum. Larger displacements result in a progression achieving its maximum intensity at later quanta, while small distortions shift the intensity toward earlier quanta.

(25) McAuliffe, C. A.; Parish, R. V.; Randall, D. P. *J. Chem. Soc., Dalton Trans.* **1979**, 1730.
(26) Tang, J.; Albrecht, A. C. *Raman Spectroscopy*; Szynanski, H., Ed.; Plenum Press: New York, 1970; Vol. 2, p. 33.
(27) Zink, J. I.; Shin, K. S. *Advances in Photochemistry*; Wiley: New York, 1991; Vol. 16, p 119.
(28) Heller, E. J. *J. Chem. Phys.* **1978**, *68*, 2066.
(29) Tannor, D. J.; Heller, E. J. *J. Chem. Phys.* **1982**, *77*, 202.
(30) Heller, E. J. *Acc. Chem. Res.* **1981**, *14*, 368.

In general displacements occur along several of the normal coordinates of the molecule. In the case where there are multiple uncoupled normal modes the total overlap is given by

$$\langle\phi|\phi(t)\rangle = \prod_k \langle\phi_k|\phi_k(t)\rangle \exp(-iE_0t - \Gamma^2t^2) \qquad (4)$$

where E_0 is the difference in the electronic energy between the minimum of the two surfaces and Γ is a damping factor. In our calculation the wave packet is displaced along the seven normal coordinates that have the largest distortions calculated from the intensities in the preresonance Raman spectrum. E_0 is taken directly from the emission spectrum as 21 655 cm^{-1}, and the value of $\Gamma = 110$ cm^{-1} is determined by the width of the vibronic bands. The ground state potential energy surface is assumed to be Gaussian and harmonic. Changes in the force constant that may occur between the ground and excited state are not treated but in general lead to very small changes.

We obtain a good fit to the experimental emission spectrum by using the seven normal modes observed in the resonance Raman spectrum and the initial displacements calculated by using the preresonance Raman intensities as discussed above. In order to achieve the best fit to the corrected experimental spectrum the displacements were modified within the experimental uncertainty (less than 10%). The uncertainty in the distortions calculated from the preresonance Raman intensities are probably larger than the purely experimental uncertainties because the emitting state is energetically in close proximity to several other states. The best calculated spectrum achieved is displayed along with the experimental spectrum in Figure 6a. Figure 6a also shows the Gaussian fit to the long-lived emission. Figure 6b displays the theoretical spectrum with the emission spectrum which was corrected by subtracting the Gaussian fit to the long lived emission. The overall shape, peak locations, and intensities in the calculated spectrum are well matched, although the experimental spectrum contains noise and is less resolved. The parameters used in calculating this spectrum are shown in Table 1.

The agreement between the Δ's calculated using the resonance Raman intensities and those that lead to a fit of the vibronic structure of the emission spectrum indicates that the distortions in the emitting state were well determined. In the excited state of **1** the major distortions occur in the Au—S stretching modes, the Au—P stretching mode, and the C═C stretching mode of the dithiolate.

IV. Relation of Δ's to the Assignment of the Emitting State. The distortions calculated above agree with the assignment of the emitting state of **1** as a LMCT involving the dithiolate ligands. The modes which are shown to be distorted in the resonance Raman and the model spectrum are those involving the gold centers and the dithiolate ligands. The Au−P bond is also distorted as expected from a change in the formal oxidation state of the gold, but no phosphine-centered modes were significantly distorted. The calculated distortions also show that there is a significant distortion in the group modes involving Au−S stretching and in the carbon−carbon stretching frequency of the dithiolate.

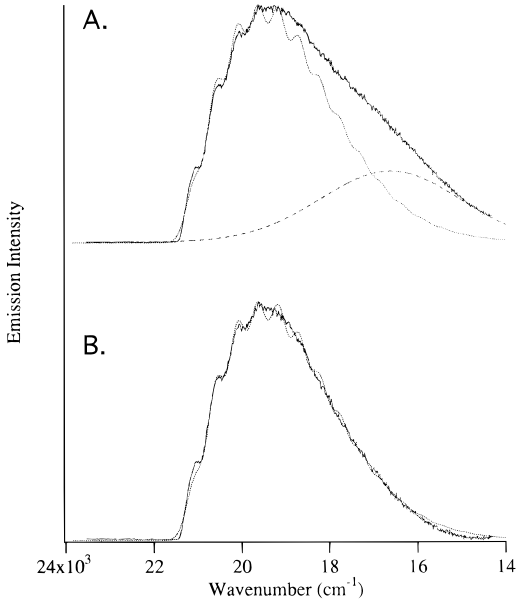

Figure 6. (a) 20 K experimental emission spectrum of **1** (solid line). Best theoretical fit to the experimental data (dotted line). Gaussian fit to the long lived emission component (dashed line). The parameters used in to obtain the fit are given in Table 1 and in the text. (b) 20 K corrected emission spectrum of **1** (solid line). The best theoretical fit to the experimental data (dotted line).

The similarity of the energies of the emission spectra of **1** and $[n\text{-}Bu_4N]_2^+$ $[Au_2(i\text{-}MNT)_2]^{2-}$ may indicate that the LMCT has a large component from the central gold atom of **1** which is in an environment similar to those in the dinuclear complex (bound on both sides to sulfur ligands). However, the fact that we observe large distortions for two Au−S modes (475 and 481 cm^{-1}) in the trinuclear gold complex that are each as large as that used to fit $(AuPPh_3)_2[i\text{-}MNT]$ indicates that all of Au−S bonds in the former are significantly perturbed. This observation shows that both the unique central gold atom and the other two gold sites may have substantial participation in the charge transfer.

Acknowledgment. This work was made possible by a grant from the National Science Foundation (CHE 91-06471), and a Laboratory Graduate Fellowship from the Department of Defense and Air Force Office of Scientific Research (S.D.H.). The authors would like to thank Prof. G. Flemming-Diaz for his helpful discussions and for use of his normal coordinate analysis of $(AuPPh_3)_2[i\text{-}MNT]$.

Supporting Information Available: Tables of crystallographic data, bond lengths and angles, atomic coordinates, and thermal parameters (4 pages). Ordering information is availible on any current masthead page.

IC951313B